Journal of Zhejiang University SCIENCE A
ISSN 1673-565X (Print); ISSN 1862-1775 (Online)
www.zju.edu.cn/jzus; www.springerlink.com
E-mail: jzus@zju.edu.cn

Investigation of a spherical-section ultrasound phased array for hepatic ablation*

ZHANG Chen-xi, CHEN Ya-zhu‡

(*Institute of Biomedical Instrument, Shanghai Jiao Tong University, Shanghai 200030, China*)

E-mail: chenxizhang@sjtu.edu.cn; yazhuchen@sjtu.edu.cn

Received Nov. 14, 2006; revision accepted Mar. 26, 2007

Abstract: A 3D ultrasound thermal model with a 3D finite element representation for modeling the thermal diffusion effects for hepatic ablation induced by spherical-section ultrasound phased array was developed. The model was first validated against available published measured data in rat liver. Using the validated model, effects of blood perfusion and heating schemes on lesion formation were studied for both single focus and split-focus intensity patterns. It was shown that for single focus sonication pattern the short-duration (~2 s) and high-intensity (~1250 W/cm^2) heating scheme can completely reduce the cooling effect of the blood perfusion. The lesion shape and size were significantly altered by perfusion for split-focus pattern even with a rapid heating scheme when the focus spacing was larger than 2.4 mm. Underdosed areas might be present between two foci. Prolonging exposure time or shortening focus spacing can reduce the cool region between two foci. In addition, the influences of thermal and acoustic parameters were also studied. When the therapy depth is short (<5 cm), the lesion size monotonically increases with increasing attenuation coefficient that ranges from 5.4 to 11 Np/(m·MHz).

Key words: Ultrasound phased-array, Blood perfusion, Temperature distribution, Numerical simulation
doi:10.1631/jzus.2007.A1237 **Document code:** A **CLC number:** Q62; Q65

INTRODUCTION

Since experimental studies using living tissue are difficult and costly, theoretical simulation of the lesion development can be extremely useful in providing a firm scientific basis for future clinical investigation of focused ultrasound. To date, numerous studies have been performed in modeling tissue heating from focus ultrasound surgery (FUS) (Kolios *et al.*, 1996; Meaney *et al.*, 1998; 2000; Curra *et al.*, 2000; Huang *et al.*, 2004; Cheng and Roemer, 2005; Persson *et al.*, 2005; Li *et al.*, 2006). In most previous models, Gaussian approximation and KZK (Khokhlov-Zabolotskaya-Kuznetsov) equation were respectively used for linear and nonlinear sound wave propagation modeling; and the Pennes bioheat transfer equation (Pennes, 1948), which was generally solved with finite difference method, was used for thermal modeling. However, few studies employed finite element method (FEM) models (Meaney *et al.*, 1998; Persson *et al.*, 2005) to investigate thermal distribution during focused ultrasound hepatic ablation, especially the thermal field of multi-focus (Sasaki *et al.*, 2003; Lu *et al.*, 2006).

The liver is a highly perfused organ, with numerous vessels throughout the liver parenchyma. These vessels might be responsible for perfusion-mediated tissue cooling and limit the size of the zone of necrosis caused by FUS ablation. Additionally, the thermal and acoustic parameters of liver may vary greatly in therapy, which may also have significant impact on the results.

The purpose of this study is to develop a 3D ultrasound thermal FEM model and quantify the influences of changes in liver blood perfusion and physical parameters for ultrasound phased-array he-

‡ Corresponding author
* Project (No. 2003CB716103) supported by the National Basic Research Program (973) of China

patic ablation. FEM excels finite difference method for predicting lesion formation because its nonuniform mesh allows for irregular boundaries, which are significant in simulations employing real organ geometry. The Rayleigh-Sommerfeld integral based method has the advantage over Gaussian approximation of being able to calculate the pressure fields for transducers of various designs, for example, transducers with a central hole for building in a B-mode ultrasound scanner.

We first presented an overview of the FE analysis of hepatic ablation using a spherical-section phased-array system. The model was then validated against available published measured data in rat liver (Chen *et al.*, 1993). Using the validated model, we performed simulations of heating in human liver tissue. We modeled two ultrasound intensity patterns in simulation: single focus and split-focus. We varied the exposure intensities and times and compared the changes of effects of blood perfusion and other liver parameters on the results.

MODELS AND METHODS

Ultrasound field calculations

A spherical-section phased-array with a radius of 200 mm was assumed in all simulation, in the center of which there was a hole where an ultrasonic imaging transducer can be built. This geometry, consisting of 89 circular elements with a radius of 8 mm which were mounted quasi-randomly on the surface in circular pattern (Li, 2001), is shown in Fig.1. The 3D field of the pressure of a circular transducer was obtained by the numerical decision of the Rayleigh-Sommerfeld integral (Mahoney *et al.*, 2001):

$$p_m = \frac{\mathrm{j}\rho ck}{2\pi}\iint_S u\frac{\mathrm{e}^{-\mathrm{j}kr}\,\mathrm{e}^{-\sum\mu_i d_i}}{r}\mathrm{d}S, \qquad (1)$$

where p_m is the complex acoustic pressure at a point m in the field, $\mathrm{j}=(-1)^{1/2}$, ρ and c are respectively the density and speed of sound in the tissue, $k=2\pi/\lambda$ is the wave number, S is the surface of the source, u is the normal velocity of the point source a, r is the distance from point source a to point m, d_i is the portion of the path from source a to point m in medium i, and μ_i is the attenuation coefficient including absorption and scattering in medium i. For an array consisting of N elements, Eq.(1) can be written as

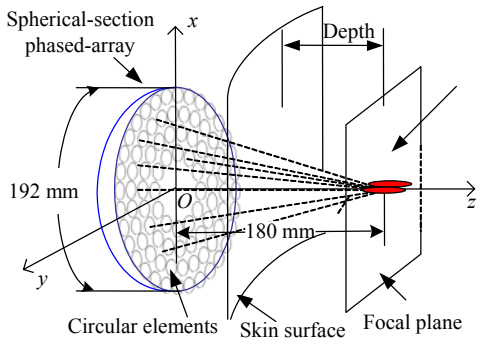

Fig.1 Geometry of the spherical-section phased array and treatment volume

$$p_m = \frac{\mathrm{j}\rho ck}{2\pi}\sum_{n=1}^{N}u_n\iint_{S_n}\frac{\mathrm{e}^{-\mathrm{j}kr_{mn}}\,\mathrm{e}^{-\sum\mu_i d_{mn,i}}}{r_{mn}}\mathrm{d}S_n, \qquad (2)$$

where S_n and u_n are, respectively, the surface and the particle velocity of the nth element of the array, r_{mn} is the distance from a point source a on the nth element to the field point m, and $d_{mn,i}$ is the portion of the path from source a on the nth element to point m in medium i. The ultrasound model was assumed to be a simple water-liver tissue model, because the effect of tissue layers on the ultrasound field is small and can be ignored (Fan and Hynynen, 1992; 1994). The surface of the circular transducer was assumed to uniformly radiate acoustic energy. The pseudoinverse acoustic pattern synthesis method (Ebbini and Cain, 1989) was used to determine the complex vector of driving signals of the phased-array to produce desired field levels at a set of control points in the treatment volume. The focal plane was located 180 mm from the center of the arrays because the maximum intensity gain can be obtained at this point under the configuration mentioned above (Li, 2001). During the simulation of split-focus, the focus spacing was initially set to 2.4 mm (center to center). The intended pressure amplitude values at all foci were identical.

Thermal modeling

1. The bioheat equation

The temperature rise in liver tissue induced by absorption of ultrasonic energy was predicted using the Pennes bioheat transfer equation (BHTE) (Pennes, 1948):

$$\rho C\frac{\partial T}{\partial t}=\nabla\cdot k\nabla T-C_{\mathrm{b}}\omega_{\mathrm{b}}(T-T_{\mathrm{b}})+Q_{\mathrm{t}}+Q_{\mathrm{m}}, \quad (3)$$

$$Q_{\mathrm{t}}=2\alpha I=\alpha\,|\,p\,|^{2}\,/(\rho c), \quad (4)$$

where ρ is the tissue density (kg/m^3), C is the tissue specific heat (J/(kg·°C)), and k is the tissue thermal conductivity (W/(m·°C)). ρ_{b} is the blood density (kg/m^3), C_{b} is the specific heat of the blood (J/(kg·°C)), ω_{b} is the blood perfusion (kg/(s·m^3)), and T_{b} is the temperature of blood. Q_{m} (W/m^3) is the energy generated by metabolic processes and was neglected as it was small. Q_{t} (W/m^3) is the absorbed power density from ultrasound. α is the US pressure absorption coefficient. The attenuation coefficient μ consists of two terms, absorption and scattering. Assuming that absorption is the main source of attenuation, the absorption coefficient was set equal to the attenuation coefficient. I is in situ spatially averaged focal intensities.

2. FEM model

We employed finite element program ANSYS 8.0 to perform all the simulations. The equation which governs the transient thermal analysis in ANSYS can be written as

$$\rho C\frac{\partial T}{\partial t}=\nabla\cdot k\nabla T+Q. \quad (5)$$

Compared with Eq.(3), Eq.(5) misses the heat sink term $\omega_{\mathrm{b}}C_{\mathrm{b}}(T-T_{\mathrm{b}})$. In previous studies concerning finite element modeling of ultrasound heating, the blood perfusion in ultrasound thermal models was absent (Meaney *et al*., 1998). The heat sink term $\omega_{\mathrm{b}}C_{\mathrm{b}}(T-T_{\mathrm{b}})$ induced by blood perfusion can be considered a process of minus heat generation which varies with temperature. Thus Q in Eq.(5) can be written as $Q(T)=Q_{\mathrm{t}}-\omega_{\mathrm{b}}C_{\mathrm{b}}(T-T_{\mathrm{b}})$, where T is time-dependent temperature of tissue, T_{b} is the temperature of blood and is assumed to be 37 °C, and Q_{t} is time-independent heat rate generated by ultrasound. Therefore, the problem of considering blood perfusion converts into the problem of solving the equation with continuous time-varying loads during FEM modeling. To specify continuous time-varying loads, we can divide the load-versus-time curve into load steps. If substeps are small enough, the load history curve can be approached by applying the loads gradually. If substeps simultaneously satisfy transient time integration rules, an accurate solution can be obtained.

A finer mesh (maximum element size 0.2 mm) was used in the target volume. Elsewhere, the mesh maximum mesh size was 8 mm. The initial temperature of the liver tissue and the temperature at the boundary of the model were set to 37 °C. The time steps during the solution of the FEM started at 0.01 s, and the maximum time step interval was 0.1 s, which is significantly less than the time constant $\tau=\rho C\delta^2/k$ for liver, with δ being the average distance between nodes. Table 1 lists the material properties used in the model, which were taken from (Valvano *et al*., 1985; Liu and Saito, 1989; Chen *et al*., 1993; Panescu *et al*., 1995). To simplify the calculations, all tissues within the computation domain were assumed to possess identical acoustic and thermal properties which remained constant during heating. Two sets of tissue properties were used in this study. Rat liver acoustic and thermal properties were used for the validation of the ultrasound thermal model and human liver tissue properties were used for FEM studies on hepatic ablation.

Table 1 The acoustic and thermal properties of rat liver used for the validation and the parameters of human liver used in FEM simulation

Parameters	Values	
	Rat liver	Human liver
Attenuation coefficient (Np/m)	20	5.4
Speed of sound (m/s)	1550	1500
Driving frequency (MHz)	1.7	1
Tissue density (kg/m^3)	1050	1060
Blood density (kg/m^3)	1060	1000
Tissue Heat capacity (J/(kg·°C))	3600	3600
Blood Heat capacity (J/(kg·°C))	3840	4180
Tissue conductive (W/(m·°C))	0.5	0.512
Perfusion rate (kg/(s·m^3))	40	Variable

3. Thermal lesion calculation

The most commonly used model for describing tissue damage is Arrhenius model defined by Sapareto and Dewey (1984), which is a function of the temperature elevation and time, and can be written as

$$EM_{43}=\int R^{(T-43)}\mathrm{d}t, \quad (6)$$

where R=2 for $T\geq$43 °C and R=4 for 37 °C<T<43 °C, T is the temperature, t is the time and EM_{43} is the thermal dose equivalence in minutes. The threshold

value of thermal dose for necrosis is EM_{43}=340 min for liver tissue (Graham *et al.*, 1999). The lesion size was then calculated from the boundaries of the thermal isodose curves generated by the simulations.

Verification of ultrasound thermal model accuracy

The accuracy of the ultrasound thermal model was first assessed through a comparison of predicted thermal lesion dimensions with published experiments data (Chen *et al*., 1993) with or without blood flow. In (Chen *et al*., 1993), thermal lesion was formed 2 mm below the surface of rat liver using a plane, 10 cm diameter piezoelectric ceramic transducer, focused using a biconcave Perspex lens. The simulated axial and transaxial full width at half pressure maximum are 1.8 mm and 18 mm respectively, which are very close to the experimental results.

RESULTS AND DISCUSSION

The measured and calculated thermal lesion diameters in rat liver are compared in Fig.2. The computed lesion dimensions agree with the experimental values fairly well and agreement is better for the unperfused cases. For the perfused case with 169 W/cm^2 I_{sal} and 20 s duration, the lesion diameter predicted by our model is 4.3 mm, while the measured lesion diameter is 5±2 mm. The model underestimated the lesion diameters by approximately 14.4%. A possible explanation of the underestimation is that micro-vasculature collapse is expected to occur during long time heating, which would have reduced the perfusion cooling effect and allowed for larger thermal lesion. In the model for validation, however, such a decrease of perfusion was not assumed.

Table 2 lists the different heating schemes used in simulation for human liver ablation. Cases I, II and III represent single focus heating pattern with I_{peak} of 1250, 833 and 500 W/cm^2, respectively. Cases IV, V and VI represent split-focus heating pattern with I_{peak} of 1250, 833 and 500 W/cm^2, respectively. For the same intensity pattern, we change the heating scheme by increasing heating duration and at the same time decreasing heating intensity so that the total absorbed energy densities (i.e. the result of absorbed power density multiplied by heating duration) were kept constant. The value used for the normal perfusion was 17.3 kg/(s·m^3), which is a mean value for human liver (Kudo *et al.*, 2004) and the value used for high perfusion rate was chosen to be 40 kg/(s·m^3) like the value used in (Kolios *et al.*, 1996).

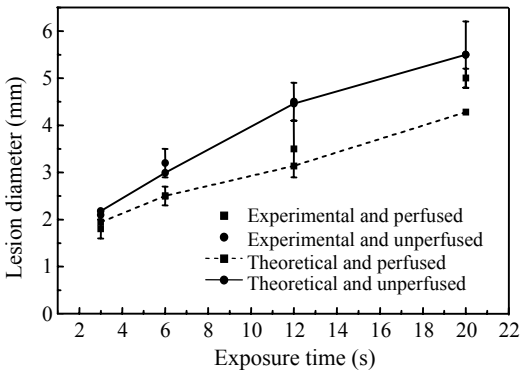

Fig.2 Comparison of measured thermal lesion diameters in perfused and unperfused rat liver (Chen *et al.*, 1993) and the corresponding results predicted by using our theoretical model. The heating intensities (I_{sal}) ranged from 67 W/cm^2 to 266 W/cm^2 and heating duration was 12 s

Fig.3 shows effects of different heating schemes on the transient temperature profiles at the focus for different blood perfusions. A higher I_{peak} leads to a sharper temperature rise followed by a faster decline immediately after the power is turned off. Under the same blood perfusion and total absorbed energy density, a more rapid heating results in a higher peak temperature. The peak temperatures shown in Fig.3 are nearly independent of the perfusion except for

Table 2 The different heating schemes used in simulation for human liver ablation

Parameters	Cases					
	I	II	III	IV	V	VI
Intensity pattern	Single focus pattern			Split-focus pattern		
In situ spatially peak intensity (I_{peak}) (W/cm^2)	1250	833	500	1250	833	500
Heating duration (s)	2	3	5	2	3	5
Absorbed power density (W/cm^3)	75	50	30	150	100	60
Total absorbed energy density (J/cm^3)	150	150	150	300	30	300

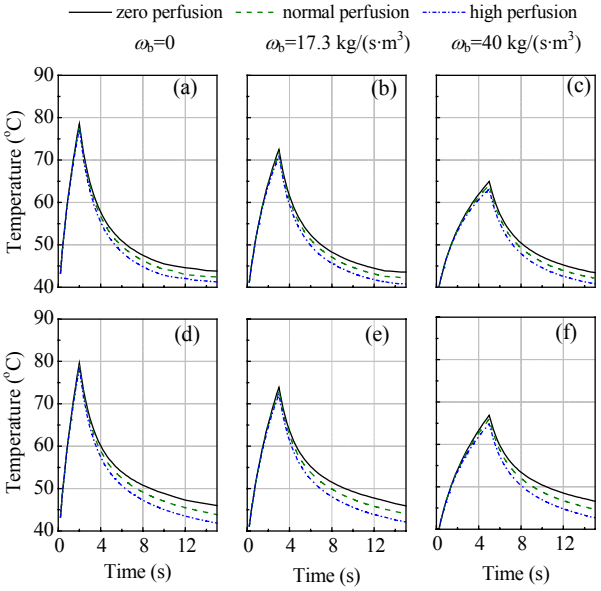

Fig.3 Effects of different heating schemes on transient temperature profiles at the focus for different blood perfusions. (a), (b), …, (f) refer to Cases I, II, …, VI respectively. Ultrasound intensity patterns were single focus for (a), (b) and (c), and split-focus for (d), (e) and (f)

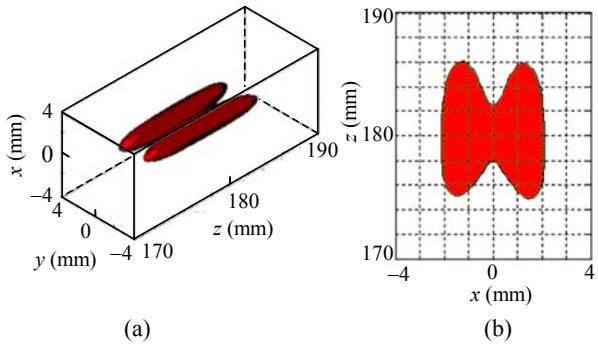

Fig.4 Threshold dose contour (EM_{43}=340 min) for split-focus pattern. Heating intensity (I_{peak}) was 1250 W/cm^2, heating duration was 2 s and blood perfusion rate was zero. (a) A perspective view of the necrosis volume; (b) 2D threshold dose contour plot in the *x*-*z* plane

Table 3 The resulting lesion diameters of different heating patterns for single focus mode

Cases	Lesion diameter (mm)		
	Zero perfusion	Normal perfusion	High perfusion
I	1.8	1.7	1.7
II	1.7	1.6	1.6
III	1.4	1.3	1.2

Cases III and VI with high perfusion. In other words, the peak temperature is significantly influenced by perfusion only if both slower heating and higher perfuion exist. An increase of perfusion according to Pennes equation reduces temperature within the target tissue. Hence, the time-varying temperature distributions of higher perfusion are lower than those of lower perfusion with the same heating scheme during the temperature decaying. Under the same blood perfusion and I_{peak}, the peak temperature for split-focus pattern is slightly larger than that for single focus pattern. This implies that heat dissipated from the focal zone is smaller for split-focus pattern than that for single focus pattern during heating.

A typical threshold dose (340 equivalent minutes at 43 °C) contour for split-focus pattern without perfusion is plotted in Fig.4. Two ellipsoid-shaped thermal lesions extend to middle and join together forming an "H"-like large lesion. In Fig.5, the influence of blood perfusion on the threshold dose contour EM_{43}=340 min for the six different heating schemes is shown. For single focus pattern, the thermal lesion outlines are similar with various inputs of perfusion and heating schemes other than the differences in size. Table 3 summarizes the characteristics of lesions for single focus pattern. It can be seen from Table 3 that the lesion diameter for Case I with normal perfusion is 1.7 mm, which is identical with that for Case I with high perfusion. The same result appears in Case II with normal and high perfusion. Whereas for Case III, the lesion diameter with high perfusion is 1.2 mm, which is reduced by 7.7% compared with the lesion made with normal perfusion. This means that variation of perfusion influences the lesion formed with longer-duration lower-intensity heating pattern more. It can also be seen from Table 3 that the long duration low-intensity heating results in a smaller lesion under the same perfusion. With zero perfusion the lesion diameter for Case III is 1.4 mm, which is reduced by 19.96% compared with the lesion (1.8 mm) for Case I. While with normal and high blood perfusion, the lesion diameter reduction rates are 22.7% and 26.7% between Cases I and III respectively. This implies that the reduction in lesion size due to long-duration low-intensity heating becomes larger with increasing perfusion.

For split-focus pattern, Figs.5d~5f show that depending on the perfusion and heating intensity, the lesion shape and size can be significantly altered. In Case IV, with high perfusion, the lesions cannot converge and keep separate in two halves. The same

results appear for Cases V and VI with normal and high perfusion. This implies that the lesion in the middle region is very sensitive to the change of perfusion. This would lead to tissue sparing during lesion forming. The possible cause for this result is that less power deposited in that region induces larger effect of perfusion. When heating intensity is small (I_{peak}<500 W/cm^2), the lesion in middle portion cannot be formed as well to link two original lesions despite zero perfusion. The reason is that there is insufficient heat from the original focal zones to be accumulated for producing efficient thermal damage. Therefore, longer exposure time and closer focus spacing are required to enlarge the join part between foci in FUS with multi-focus pattern.

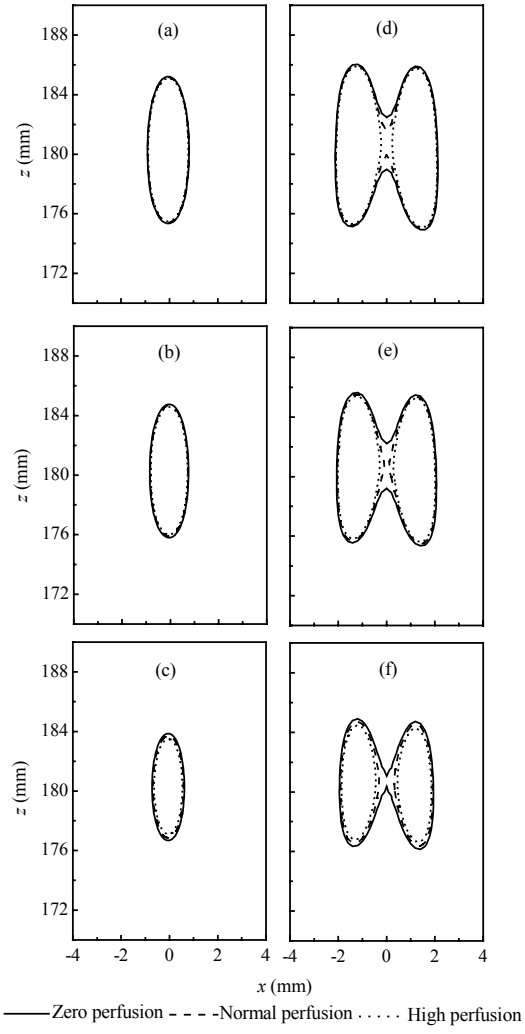

Fig.5 Effects of perfusion and different heating schemes on thermal dose equivalence EM_{43}=340 min contours at t=15 s. (a), (b), …, (f) refer to Cases I, II, …, VI, respectively

Fig.6 shows the effects of longer heating duration and closer focus spacing on the lesion formation. When the heating duration was prolonged, the effect of blood perfusion was weakened and the cooling zone between two foci shrank significantly even maintaining the initial focus spacing. While when the focus spacing was 2 mm, the effect of perfusion was not distinct even though the heating condition was the same as that for Case V. The portion which is influenced much by perfusion in split-focus pattern is the joined part between two original focal regions. Taking Fig.5e as an example, while there are slight changes in the outer lesion boundaries with various inputs of perfusion, the distortion in inner boundaries of lesions is noticeable and leads to the reduction of lesion size. The lesion formed in this region is mainly due to the heat conducted from the two original foci and a small quantity of ultrasound power deposition. Low power absorbed density in the region results in lesion forming which is highly sensitive to perfusion.

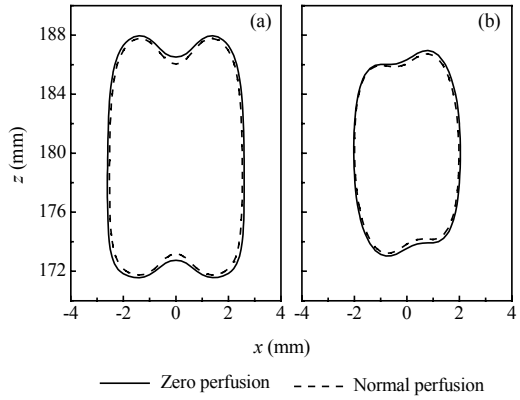

Fig.6 Effects of longer heating duration and closer focus spacing on the lesion formation with and without perfusion. (a) The heating pattern of 833 W/cm^2 I_{peak}, 6 s heating duration and 2.4 mm focal spacing; (b) The heating pattern of 833 W/cm^2 I_{peak}, 3 s heating duration and 2 mm focal spacing

The effect of change in liver thermal conductivity on lesion diameter as a function of the time for Cases I, II, III is shown in Fig.7. The conductivity is varied by ±50% from 0.512 W/(m·°C) and the perfusion is chosen to be zero. Under the same power deposition, a lower thermal conductivity results in a larger lesion. When absorbed power density is constant, low conductivity slows down the heat dissipating from the focal region, leads to more heat ac-

cumulation in focal region at the unit duration and forming a larger lesion. Effects of the change of conductivity become larger with the decreasing absorbed power density (i.e. I_{peak}). When absorbed power density is 50 W/cm^3 (Case III), the lesion diameters are changed by −35.5% and 27.3% for k=0.768 and 0.216 W/(m·°C) respectively. While for absorbed power density of 75 W/cm^3 (Case I), the changes are only −8.57% and 8.21%. The same results appear for split-focus pattern as shown in Fig.8, which illustrates the effects of thermal conductivity on the domain of thermal lesion (EM_{43}=340 min) for Cases IV, V and VI. When k is 0.768 W/(m·°C), the lesions are not only kept separate but also shrink largely for Cases V and VI. The distinction between

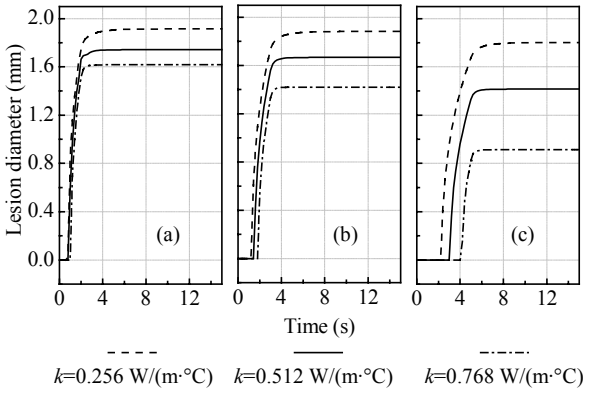

Fig.7 Influence of the heat conductivity on the rate of lesion diameter change for single focus pattern heating. (a), (b), (c) refer to Cases I, II, III, respectively. The perfusion is zero and Cases I, II and III are illustrated in Table 2

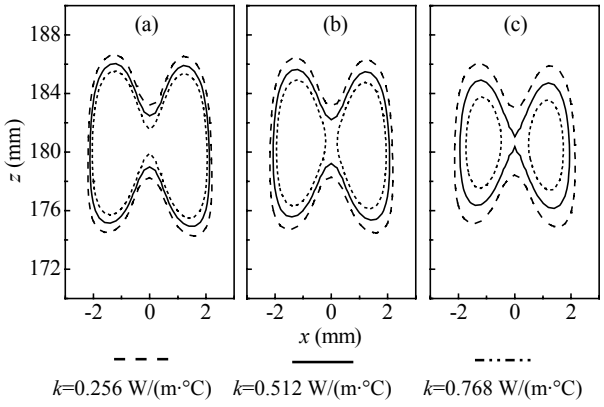

Fig.8 Effects of thermal conductivity on thermal dose equivalence EM_{43}=340 min contours for split-focus pattern heating. (a), (b), (c) refer to Cases IV, V, VI, respectively. The perfusion is zero and the heating Cases IV, V and VI are illustrated in Table 2

effects of perfusion and conductivity for split-focus heating pattern is that the effect of perfusion acts on the lesion in the joined part between two original foci, while the effect of conductivity acts on the whole lesion which combines two original foci.

The attenuation coefficient was initially set to 5.4 Np/(m·MHz) according to the values offered by Liu and Saito (1989). However, the value of attenuation coefficient in tissue may vary with temperature or under exposure of high intensity ultrasound as suggested by (Gertner *et al.*, 1997; Zderic *et al.*, 2004). Therefore, the effect of ultrasound attenuation on the lesion diameter was studied. We performed the simulations with the attenuation varying by 200% and −50% from 5.4 Np/(m·MHz), exposure time of 2 s and zero perfusion. The output acoustic power was chosen so that with initial value of 5.4 Np/(m·MHz) the I_{peak} was 1250 W/cm^2 (Case I) with various inputs of therapy depth. The output power used to elevate the I_{peak} to 1250 W/cm^2 must be increased for deeper exposure. The therapy depth was the distance from the center of target volume to the skin surface (see Fig.1). In Fig.9, the lesion diameter of single focus heating pattern is shown as a function of ultrasound attenuation with therapy depth of 2.5 cm, 5 cm, 7.5 cm and 10 cm. It can be observed that lesion diameters first increase and then decrease with the increasing attenuation coefficient. The turning points of the function curve for different therapy depth change significantly. When therapy depth is 5 cm, the maximum lesion was obtained with the attenuation coefficient between 8.1 and 13.5 Np/(m·MHz). When therapy depth is 10 cm, the maximum lesion was obtained with the attenuation coefficient between 2.7 and 8.1 Np/(m·MHz). The influence of ultrasound attenuation on the lesion for split-focus pattern is similar to that of the thermal conductivity. In our model, we assumed that the ultrasound attenuation coefficient is equal to the absorption coefficient. Ultrasound attenuation and absorption act oppositely for lesion generation according to Eqs.(2) and (4). Small attenuation coefficient would result in lower prefocal ultrasound energy deposition and greater ultrasound intensity in the focal region (Eq.(2)). On the contrary, small absorption coefficient would result in lower power absorption of tissue according to Eq.(4). Therefore, the lesion size would not increase or decrease with increasing attenuation coefficient mono-

tonically. For a certain therapy depth, there would be a certain value of attenuation coefficient as a compromise for attenuation and absorption with which the largest lesion can be obtained.

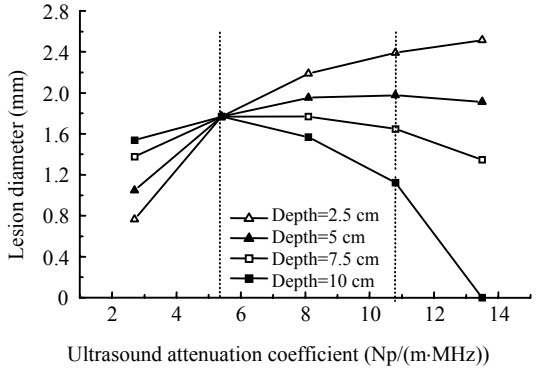

Fig.9 The lesion diameter as a function of the attenuation coefficient for single focus pattern. The simulations were made for 2 s of ultrasound exposure with zero perfusion

CONCLUSION

The ultrasound thermal model with 3D finite element representation of bioheat equation has been successfully employed to predict the shape and size of ultrasonically induced lesions. For single focus sonication pattern, the short-duration (~2 s) and high-intensity (~1250 W/cm^2) heating scheme can completely reduce the cooling effect of the blood perfusion. However, for multi-focus sonication pattern, the lesion shape and size would be changed distinctly for normal perfusion (17.3 kg/(s·m^3)) even with a rapid heating scheme when the focus spacing was larger than 2.4 mm. Underdosed areas might be present between two foci from which the tumor can regenerate. Prolonging exposure time or shortening focus spacing can reduce the cool region between two foci. Within the range of possible ultrasound attenuation coefficient (5.4~11 Np/(m·MHz)), when the therapy depth is short (<5 cm), the lesion size increases with increasing attenuation coefficient monotonically; whereas when the therapy depth is long, the lesion size decreases with increasing attenuation coefficient monotonically.

References

Chen, L.L., ter Haar, G.R., Hill, C.R., Dworkin, M., Carnochan, P., Young, H., Bensted, J.P.M., 1993. Effect of blood perfusion on the ablation of liver parenchyma with high-intensity focused ultrasound. *Phys. Med. Biol.*, **38**(11):1661-1673. [doi:10.1088/0031-9155/38/11/011]

Cheng, K.S., Roemer, R.B., 2005. Blood perfusion and thermal conduction effects in Gaussian beam, minimum time single-pulse thermal therapies. *Med. Phys.*, **32**(2):311-317. [doi:10.1118/1.1835591]

Curra, F.P., Mourad, P.D., Khokhlova, V.A., Cleveland, R.O., Crum, L.A., 2000. Numerical simulations of heating patterns and tissue temperature response due to high-intensity focused ultrasound. *IEEE Trans. on Ultrason. Ferroelectr. Freq. Control*, **47**(4):1077-1088. [doi:10.1109/58.852092]

Ebbini, E.S., Cain, C.A., 1989. Multiple-focused ultrasound phased-array pattern synthesis: optimal driving-signal distributions for hyperthermia. *IEEE Trans. on Ultrason. Ferroelectr. Freq. Control*, **36**(5):540-548. [doi:10.1109/58.31798]

Fan, X., Hynynen, K., 1992. The effect of wave reflection and refraction at soft tissue interfaces during ultrasound hyperthermia treatments. *J. Acoust. Soc. Am.*, **91**(3):1727-1736. [doi:10.1121/1.402452]

Fan, X., Hynynen, K., 1994. The effects of curved tissue layers on the power deposition patterns of therapeutic ultrasound beams. *Med. Phys.*, **21**(1):25-34. [doi:10.1118/1.597250]

Gertner, M.R., Wilson, B.C., Sherar, M.D., 1997. Ultrasound properties of liver tissue during heating. *Ultrasound in Med. & Biol.*, **23**(9):1395-1403. [doi:10.1016/S0301-5629(97)00150-6]

Graham, S.J., Chen, L., Leitch, M., Peters, R.D., Bronskill, M.J., Foster, F.S., Henkelman, R.M., Plewes, D.B., 1999. Quantifying tissue damage due to focused ultrasound heating observed by MRI. *Magn. Reson. Med.*, **41**(2):321-328.

Huang, J.L., Holt, R.G., Cleveland, R.O., Roy, R.A., 2004. Experimental validation of a tractable numerical model for focused ultrasound heating in flow-through tissue phantoms. *J. Acoust. Soc. Am.*, **116**(4):2451-2458. [doi:10.1121/1.1787124]

Kolios, M.C., Sherar, M.D., Hunt, J.W., 1996. Blood flow cooling and ultrasonic lesion formation. *Med. Phys.*, **23**(7):1287-1298. [doi:10.1118/1.597694]

Kudo, M., Murakami, T., Hashimoto, K., Hori, M., Kim, T., Nakamura, H., 2004. Comparison of the Hepatic Perfusion Parameters in Patients with Normal and Chronic Liver Disease. 90th Scientific Assembly and Annual Meeting of the RSNA. Chicago.

Li, G.W., 2001. Research of High Intensity Focused Ultrasound Phased Array and Treatment Thermal Field. Ph.D Thesis, Shanghai Jiao Tong University, China (in Chinese).

Li, F., Feng, R., Zhang, Q., Bai, J., Wang, Z., 2006. Estimation of HIFU induced lesions in vitro: numerical simulation and experiment. *Ultrasonics*, **44**(S1):337-340. [doi:10.1016/j.ultras.2006.07.002]

Liu, D.L., Saito, M., 1989. A new method for estimating the acoustic attenuation coefficient of tissue from reflected ultrasonic signals. *IEEE Trans. on Med. Imaging*, **8**(1):107-110. [doi:10.1109/42.20371]

Lu, M., Wan, M., Xu, F., Wang, X., Chang, X., 2006. Design and experiment of 256-element ultrasound phased array for noninvasive focused ultrasound surgery. *Ultrasonics*, **44**(S1):325-330. [doi:10.1016/j.ultras.2006.07.015]

Mahoney, K., Fjield, T., McDannold, N., Clement, G., Hynynen, K., 2001. Comparison of modelled and observed *in vivo* temperature elevations induced by focused ultrasound: implications for treatment planning. *Phys. Med. Biol.*, **46**(7):1785-1798. [doi:10.1088/0031-9155/46/7/304]

Meaney, P.M., Clarke, R.L., ter Haar, G.R., Rivens, I.H., 1998. A 3-D finite-element model for computation of temperature profiles and regions of thermal damage during focused ultrasound surgery exposures. *Ultrasound in Med. & Biol.*, **24**(9):1489-1499. [doi:10.1016/S0301-5629(98)00102-1]

Meaney, P.M., Cahill, M.D., ter Haar, G.R., 2000. The intensity-dependence of lesion position shift during focused ultrasound surgery. *Ultrasound in Med. & Biol.*, **26**(3):441-450. [doi:10.1016/S0301-5629(99)00161-1]

Panescu, D., Whayne, J.G., Fleischman, S.D., Mirotznik, M.S., Swanson, D.K., Webster, J.G., 1995. Three-dimensional finite element analysis of current density and temperature distribution during radio-frequency ablation. *IEEE Trans. on Biomed. Eng.*, **42**(9):879-890. [doi:10.1109/10.412649]

Pennes, H.H., 1948. Analysis of tissue and arterial blood temperatures in the resting human forearm. *J. Appl. Phys.*, **1**(2):93-122.

Persson, J., Hansen, E., Lidgern, L., McCarthy, I., 2005. Modeling of the heat distribution in the intervertebral disk. *Ultrasound in Med. & Biol.*, **31**(5):709-717. [doi:10.1016/j.ultrasmedbio.2005.01.018]

Sapareto, S.A., Dewey, W., 1984. Thermal dose determination in cancer. *Int. J. Radiat. Oncol. Biol. Phys.*, **10**(6):787-800.

Sasaki, K., Azuma, T., Kawabata, K.I., Shimoda, M., Kokue, E.I., Umemura, S.I., 2003. Effect of split-focus approach on producing larger coagulation in swine liver. *Ultrasound in Med. & Biol.*, **29**(4):591-609. [doi:10.1016/S0301-5629(02)00792-5]

Valvano, J.W., Cochran, J.R., Diller, K.R., 1985. Thermal conductivity and diffusivity of biomaterials measured with self-heating thermistors. *Int. J. Thermophys.*, **6**(3):301-311. [doi:10.1007/BF00522151]

Zderic, V., Keshavarzi, A., Andrew, M.A., Vaezy, S., Martin, R.W., 2004. Attenuation of porcine tissues *in vivo* after high intensity ultrasound treatment. *Ultrasound in Med. & Biol.*, **30**(1):61-66. [doi:10.1016/j.ultrasmedbio.2003.09.003]